Intermediate mass fragment emission in Fe+Au collisions

T. C. Sangster, H. C. Britt, D. J. Fields, L. F. Hansen, R. G. Lanier, M. N. Namboodiri, B. A. Remington, and M. L. Webb*
Lawrence Livermore National Laboratory, Livermore, California 94550

M. Begemann-Blaich,† T. Blaich,‡ M. M. Fowler, and J. B. Wilhelmy
Los Alamos National Laboratory, Los Alamos, New Mexico 87545

Y. D. Chan, A. Dacal,§ A. Harmon,** J. Pouliot,†† and R. G. Stokstad
Lawrence Berkeley Laboratory, Berkeley, California 94720

S. Kaufman and F. Videbaek‡‡
Argonne National Laboratory, Argonne, Illinois 60439

Z. Fraenkel
Weizmann Institute of Science, 76100 Rehovot, Israel

G. Peilert, H. Stöcker, and W. Greiner
Institut fur Theoretische Physik der Universität, Frankfurt, Germany

A. Botvina and I. N. Mishustin
Institute for Nuclear Research, Moscow 117312, Russia
(Received 14 October 1991)

Experimental results are presented on the charge, velocity, and angular distributions of intermediate mass fragments (IMFs) for the reaction Fe+Au at bombarding energies of 50 and 100 MeV/nucleon. Results are compared to the quantum molecular dynamics (QMD) model and a modified QMD which includes a Pauli potential and follows the subsequent statistical decay of excited reaction products. The more complete model gives a good representation of the data and suggests that the major source of IMFs at large angles is due to multifragmentation of the target residue.

PACS number(s): 25.70.Mn

I. INTRODUCTION

The emission of intermediate mass fragments (IMF, $A \approx 6-50$) is an important probe of the dynamical evolution and final state coalescence or freeze-out in heavy ion reactions at medium energies (20–200 MeV/nucleon). At low energies (<20 MeV/nucleon) IMF emission is a rare process [1] while at high energies (>1 GeV/nucleon), the reactions are so violent that in a central collision most emission products are nucleons and pions [2]. In the transition region, experiments [3–11] with heavy systems involving a wide range of projectile/target mass ratios have suggested that the most important parameter in IMF emission is the total energy deposition, $E_{\rm dep}$, in the heavy target residue. Empirically, the IMF multiplicity shows a steep rise [6] in the region $E_{\rm dep} \sim 2-5$ MeV/nucleon, an approximate plateau region above 5 MeV/nucleon and then falls off again [9] for $E_{\rm dep} > 10$ MeV/nucleon. These results are consistent with measurements of the relative population of widely separated states in Li and Be fragments [10,11] which suggest a limiting temperature of ~ 6 MeV for the IMF source. The saturation of nucleon emission [12,13] in Ar and Kr reactions is also consistent with a limiting energy deposition in the interaction region.

In these reactions there appear to be two major sources of IMFs. The first comes from the dynamical correlation established in the very early stages of the collisions [14,15]. The second is from the statistical fragmentation [16–24] of highly excited heavy residues at the "freeze-out" stage of the reaction. For early times in the reaction the quantum molecular dynamics approach (QMD) [14,15] has had considerable success in describing the ini-

*Present address: Dynamics Technology, 21311 Hawthorne Blvd., Torrance, CA 90503.
†Present address: Gesellschaft für Schwerionenforschung, KP 3, Postfach 11 05 52, D-61 Darmstadt, Germany.
‡Present address: Universität Mainz, Institut für Kernchemie, D-65 Mainz, Germany.
§Present address: Instituto De Fisica, UNAM, Mexico, DF 01000, Mexico.
**Present address: Space Science Lab., NASA-Marshall Space Flight Center, Huntsville, AL 35812.
††Present address: Laboratoire de Physique, Nucleaire, Universite Laval Ste Foy, Quebec, GIK7P4, Canada.
‡‡Present address: Brookhaven National Laboratory, Physics Dept., Bldg. 901A, Upton, NY 11973.

tial collision and the approach to thermalization in the residues. Because the QMD model explicitly treats the nucleon correlation information throughout the time evolution of the collision, it is able to describe the fluctuations that lead to the final fragmentation of the nuclear system. This is a major improvement over the mean-field models which can describe only average properties of the collisions and do not contain the explicit correlations necessary to create complex fragments. However, at later stages of the reaction the QMD has difficulties because of the two time scales involved; initial hot fragment formation occurs typically during the collision time ($\sim 10^{-22}$ sec) while evaporation (cooling) may take up to 10^{-16} sec. Furthermore, in ordinary QMD the excitation energies of the emitted fragments are not well enough determined to follow their subsequent statistical decay at late times with sufficient precision.

Complementary models [16–24] have been developed to describe the multifragmentation of the residual nuclear system in terms of either a statistical breakup [16–20], which may involve passage through the nuclear equivalent of a liquid-gas phase transition, or the sequential evaporation of IMFs [21,22]. These models are informative but are generally not directly comparable to experiment because of the unrealistic initial conditions. A chemically and thermally equilibrated, spherical source with an appropriate laboratory velocity boost is often taken for the initial condition. Recently, more complete models have used an intranuclear cascade (INC) description or the Vlasov-Uehling-Uhlenbeck (VUU) model for the initial stages of the interaction and a statistical deexcitation at later stages. This approach has been used to describe IMF production in p-nucleus collisions [19] and heavy ion collisions [23,24] and also fission following peripheral collisions for Fe+Au bombardments [25]. The INC and VUU approaches do not, however, contain the dynamical correlations necessary to describe multifragmentation in central heavy ion collisions.

In this paper, we present data on IMF production with Fe projectiles in the 50–100 MeV/nucleon transition region and compare the results with QMD calculations. The comparisons suggest the need to include late time fragment deexcitation to the QMD approach and first results of attempts in this direction are presented.

II. EXPERIMENTAL

A. Setup and particle identification

The experiment was performed using 50 and 100 MeV/nucleon Fe beams from the LBL Bevalac accelerator and the PAGODA detector array [26]. The detector layout and an individual PAGODA module are shown schematically in Fig. 1. The eight modules are mounted symmetrically around a target chamber at polar angles of 36°, 72°, 108°, and 144° and subtend approximately 26° in both θ and ϕ for a total solid angle slightly greater than 10% of 4π. Each module is a composite detector consisting of two position-sensitive multiwire proportional counters (MWPCs), a low pressure proportional counter (PC), a high pressure, axial field ionization chamber (IC), and a nine-element fast-slow plastic phoswich array.

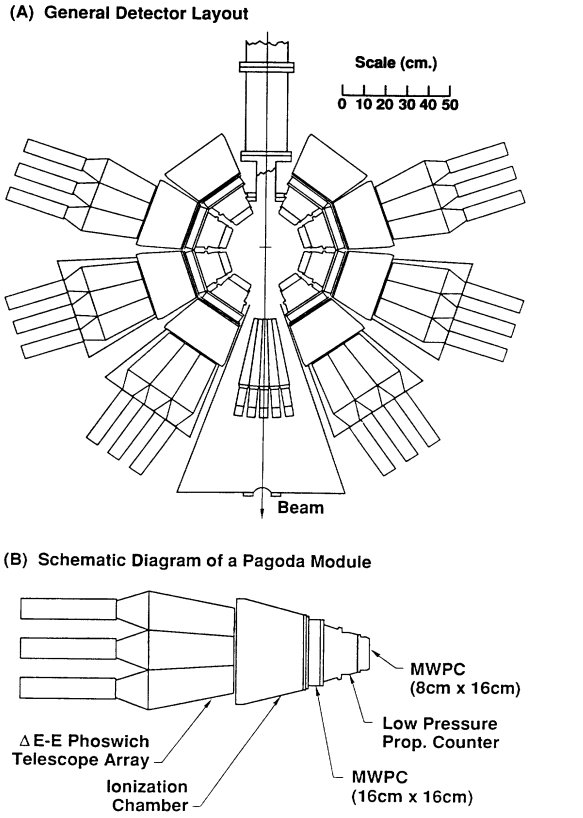

FIG. 1. A schematic diagram of (a) the detector layout and of (b) an individual PAGODA module.

Final fragment identification consists of nuclear charge (Z), position (θ,ϕ), and incident velocity (V). For fragments with $Z \geq 4$ and $V \leq 4.1$ cm/nsec, velocities and positions are obtained using timing and position information from the two MWPCs. For $V > 2.5$ cm/nsec, the phoswich modules provide the fragment energy and within the approximately 8° granularity of each module in both θ and ϕ, the fragment position. Estimates for the fragment charge are made by comparing the responses of various PAGODA elements to systematic calibration data. The calibration data has been used [27] to construct two-dimensional masks of PC vs TOF (time of flight), IC vs TOF, IC vs phoswich fast plastic (FP) ΔE, and phoswich ΔE vs E for Z identification. In addition, a second PC vs TOF mask also provides the incident fragment velocity. The final charge assignment typically involves more than one of the identification masks. At backward angles, virtually all IMFs with $Z \geq 3$ can be identified using the IC or PC mask. The only effective measurement threshold is the several hundred keV/nucleon required to reach the second MWPC. The efficiency corrections are generally quite small as well. At forward angles, however, the peak in the IMF energy distribution puts the bulk of the fragments into the fast plastic. The initial fragment charge obtained from the PC vs TOF mask is generally not as reliable for the lighter fragments and is used only if values are not available from the FP vs TOF or IC vs TOF masks. If the PC value differs significantly from the IC or FP (three or

more units), this is a good indication that more than one charged particle ($Z > 1$) passed through the module.

Multiple charged particles in the 36° modules account for approximately 50% of the MWPC triggers. An algorithm has been developed to handle these events in which fully identified fragments or alphas (protons are ignored) in the phoswich detectors are used to adjust the PC and IC pulse heights and new Z values generated from the masks. The basic assumption is that the multiple events involve only one fragment which triggers the MWPCs and one or more lighter particles in the phoswich detectors. The new Z values are compared and a final gas Z is assigned to the MWPC trigger as though the module contained a single fragment.

The charge resolution of the various identification masks for the IMFs ($2 \leq Z < 18$) is generally quite good. The single fragment resolution of the two IC masks is unity while the resolution of the PC-TOF depends significantly on the fragment velocity and charge. We estimate that the overall IMF charge resolution for all events is close to unity for $Z < 10$, approximately two units for fragments with $10 \leq Z \leq 20$, and two to three units for fragments in the fission-mass region. The velocity resolution of the original PC-TOF calibration is 0.05 cm/ns between 0.5 and 2.4 cm/ns (there is some Z dependence on the range of the calibration data). Using the measured TOF, the velocity calibration has been extended to 4.1 cm/ns with comparable resolution.

B. Efficiency corrections and cross sections

In order to make estimates of absolute cross sections for IMF yields it is necessary to know the efficiencies of the detection techniques as a function of Z and V. The primary fragment triggers for the PAGODA modules are based on the MWPCs and the phoswich detectors. For fragments with $Z > 10$, the MWPC anode and position efficiencies are close to unity. For $Z = 2,3$ the MWPCs are very inefficient and the identification is done with the phoswich detectors with a velocity threshold of 2.5 cm/nsec. In the intermediate region, $Z = 4-10$, the MWPC efficiencies vary significantly with Z and V.

Since the MWPC anode efficiency is reasonably high for $Z \geq 4$, we decided to use only the MWPC trigger data to estimate the yield of these fragments using efficiencies generated by comparing singles yields in the phoswich detectors with the corresponding yield in the MWPCs for fragments with velocities above 2.5 cm/nsec. Our trigger setup seriously limits the statistical accuracy for phoswich triggers with $Z \geq 4$ and we are, therefore, limited to a velocity integrated efficiency above 2.5 cm/nsec for each Z. Due to a lack of more detailed information we assumed a simple linear dependence for the efficiency as a function of V. This function assumed the measured value for each Z was appropriate for the average V in the phoswich modules and that the efficiency was unity at $V = 0$. Our estimate is that this simple procedure is accurate to about ±25% of the correction and this has been included in the error bars for the data presented. Figure 2 shows the average MWPC anode efficiencies for $V > 2.5$ cm/nsec as a function of Z for the two forward modules.

The MWPC position measurements are somewhat less efficient than the anode triggers but the data set gives a direct measure of the position versus anode efficiencies as a function of V,Z. We use these measured efficiencies along with the estimated anode efficiencies discussed above to obtain absolute IMF yields.

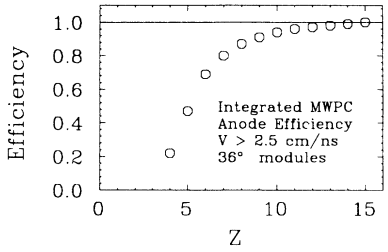

FIG. 2. Average velocity integrated anode efficiency as a function of fragment charge for the forward two modules. The fragments were required to reach the phoswich detectors which have a threshold of approximately 2.5 cm/nsec.

The beam flux during the experiment was monitored by an ion chamber located downstream from the target chamber. Periodic calibrations were made during the experiment using a scintillator paddle to count single beam particles and particle yield ratios have since been calculated as a function of calibrated beam flux. These ratios fluctuate somewhat during the experiment and form the basis for an estimated 20% systematic uncertainty in the overall cross section measurement.

We have corrected the data for the transmission of the MWPCs, the support mesh for the ion chamber window, and the ion chamber Frisch grid. We have corrected all events for the full transmission of each MWPC (94%) and, for those fragments identified using the IC or phoswich detectors, the IC window mesh (88%), and the Frisch grid (90%).

The data was taken with a 1.34 mg/cm^2 Au target. The 100 MeV/nucleon Fe+Au data were taken with the target oriented 45° to the beam while the 50 MeV/nucleon data were taken with the target perpendicular to the beam. Since only slight differences have been observed in the velocity distributions of the heaviest fragments, no attempt has been made to correct the IMF yields for the different target orientations except to account for the increased target thickness when calculating cross sections.

III. EXPERIMENTAL RESULTS

In this section we present inclusive and semiexclusive distributions for intermediate mass fragments with $2 \leq Z \leq 50$.

In inclusive distributions it is not possible to unambiguously separate fission-mass fragments due to multifragmentation in central collisions from true binary fission of the target residue in peripheral reactions. However, from correlations with projectile fragments and associated proton multiplicities we have made the following conclusions [4,27]. Intermediate mass fragments ($Z < 20$) come almost exclusively from multifragmentation in central collisions. The coincident light particle multiplicities in the

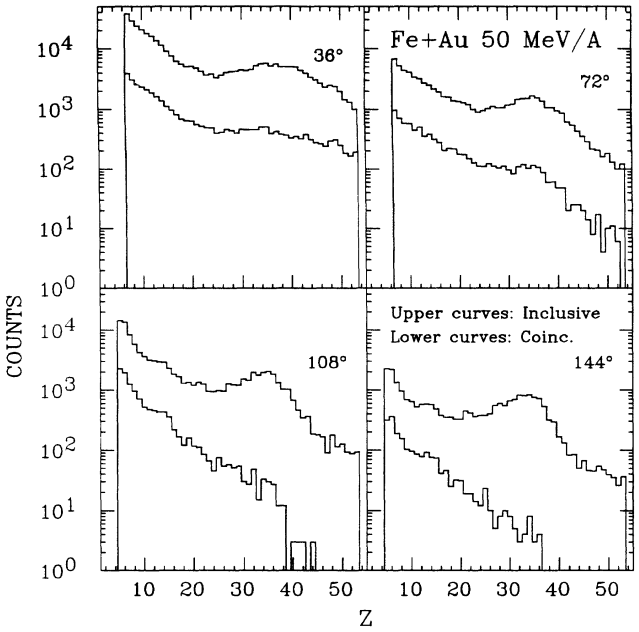

FIG. 3. Measured intermediate mass fragment charge distributions at laboratory angles of 36°, 72°, 108°, and 144° for the 50 MeV/nucleon Fe+Au system. The coincidence distributions have the requirement that an additional IMF ($Z<20$) was detected in any other PAGODA module. These distributions have not been corrected for MWPC efficiency.

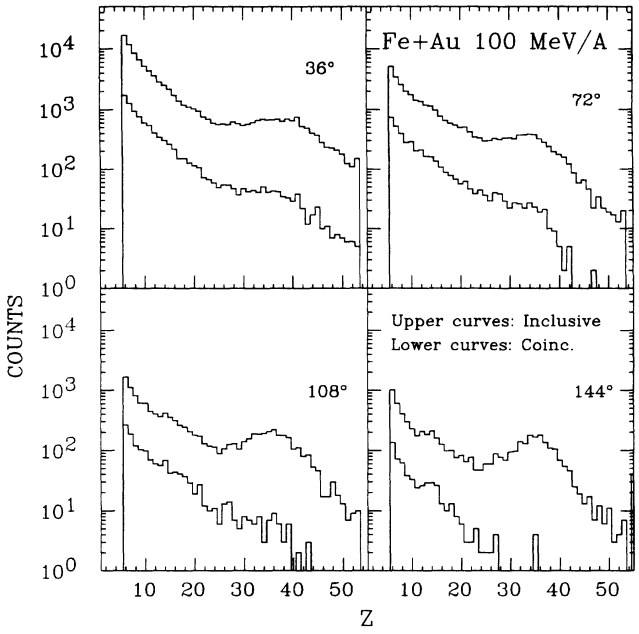

FIG. 4. Same as Fig. 3 for the 100 MeV/nucleon Fe+Au system.

phoswich arrays are significantly larger than for any other class of event and there are very few large projectile fragments observed in the forward hodoscope. In the fission mass region ($Z>20$), there are contributions from both binary fission and multifragmentation. The light particle multiplicities are only somewhat lower while the charge distribution of the heaviest fragment in the forward hodoscope is bimodal; the lower Z peak corresponds closely with the one for IMF production and the higher Z peak matches exactly the distribution observed for purely binary fission. Finally, coincidences between two fragments with $Z>20$ clearly isolates fission events [27], whereas a coincidence in which at least one fragment has $Z<20$ is almost always a central multifragmentation event. A similar effect and characterization has been observed previously in the Ne+Au reaction at 200 MeV/nucleon by Warwick *et al.* [7].

In Figs. 3 and 4 we show both inclusive and coincidence Z spectra. The coincident spectra correspond to the condition where a fragment in the indicated angular bin is in coincidence with another fragment $5\leq Z\leq 20$, in any of the other seven detector modules. Relative coincidence rates (shown for the 100 MeV/nucleon reaction in Table I) and previously published correlations [4,25,27] with the forward hodoscope show that this coincidence virtually eliminates the contribution from binary fission. In contrast, the probability of finding two light fragments and a third fragment within our acceptance is quite high.

In Figs. 5 and 6 we show differential cross sections $d\sigma(Z)/d\Omega$ as a function of laboratory angle. The cross sections shown are an integral over the velocity distribu-

TABLE I. Relative coincidence rates for various fragment combinations with $Z_L=5$–20 and $Z_H=21$–53. Results are summed over the total acceptance of the detector.

Event type	Yield (100 MeV/nucleon)		Yield (50 MeV/nucleon)	
Total	352 105		318 553	
L	188 952	53.7%	122 764	38.5%
H	84 176	23.9%	112 793	35.4%
$L\times L$	56 660	16.1%	52 883	16.6%
$L\times H$	6990	2.0%	11 222	3.5%
$H\times H$	5291	1.5%	8451	2.7%
$L\times L\times L$	7261	2.1%	5571	1.7%
$L\times L\times H$	1493	0.4%	3593	1.1%
$H\times H\times L$	38	0.0%	178	0.0%
$H\times H\times L+$	10	0.0%	33	0.0%
$L\times L\times L+$	1234	0.3%	1065	0.3%

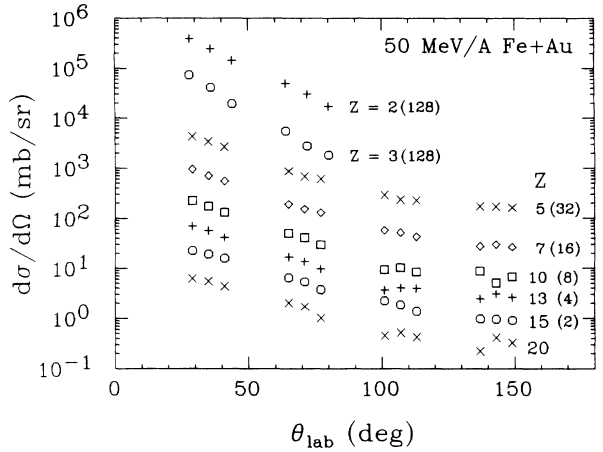

FIG. 5. Experimental IMF angular distributions in the laboratory for the 50 MeV/nucleon Fe+Au reaction. The numbers in parentheses are multiplicative offsets for display.

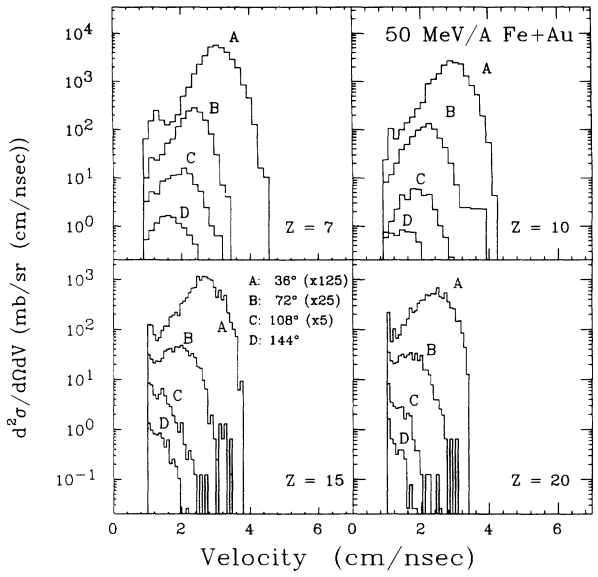

FIG. 7. Experimental velocity distributions for $Z=7$, 10, 15, and 20 at the four primary detector angles for the 50 MeV/nucleon Fe+Au reaction.

tion above a low energy cutoff of 1.0 cm/nsec. These velocity distributions are shown in Figs. 7 and 8. Here we see that only for $Z>10$ at backward angles is there significant cross section below this low energy cutoff. Figures 9 and 10 show the same data in a two-dimensional plot of the invariant cross section as a function of $P_\perp$ and $P_\parallel$ for $Z=7$ and $Z=15$. From these figures we can see that there is no obvious single moving frame that can be used to characterize the data. Thus, it is not possible to reliably estimate a total yield for each Z and we have instead chosen to report only the integral above our low energy cutoff.

The angular distributions are peaked forward with slopes decreasing with increasing Z. For the highest Z values the observed cross sections at backward angles are significantly lower than the total cross section due to the loss of events below our low energy cutoff. The relatively large cross sections and almost isotropic distributions at large angles suggest qualitatively that emission from a slow moving target residue is an important source of IMFs in these reactions.

IV. QMD MODEL

The original QMD approach, which is described in detail in Refs. [14,15,28–30], incorporates the important quantum features of the Vlasov-Uehling-Uhlenbeck (VUU) theory [31–40], namely, the Pauli principle, stochastic scattering, and particle production, into the N-body phase space dynamics of the classical molecular dynamics method [41–49].

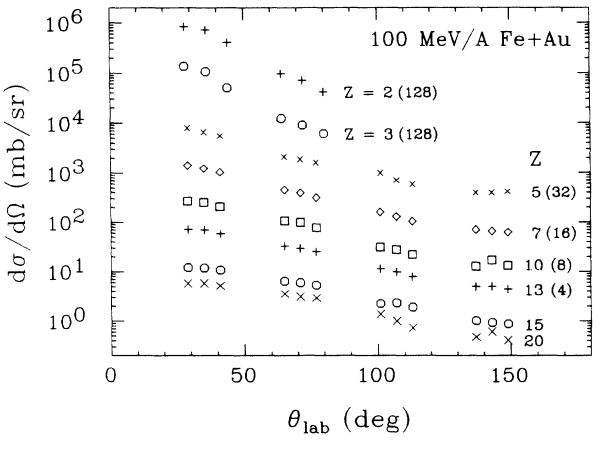

FIG. 6. Same as Fig. 5 for the 100 MeV/nucleon Fe+Au reaction.

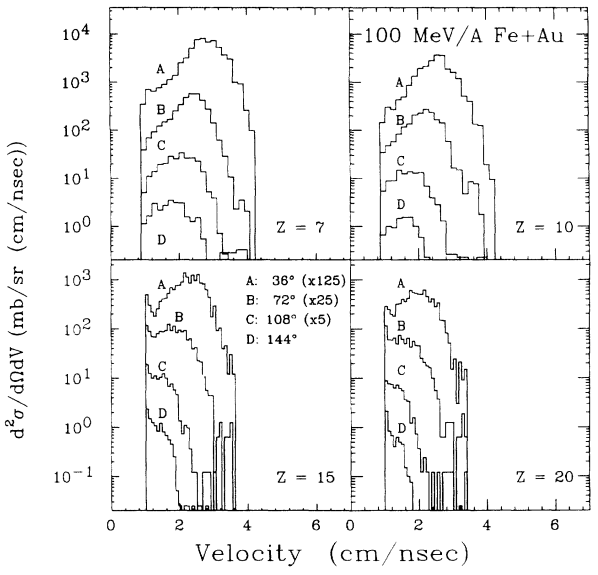

FIG. 8. Same as Fig. 7 for the 100 MeV/nucleon Fe+Au reaction.

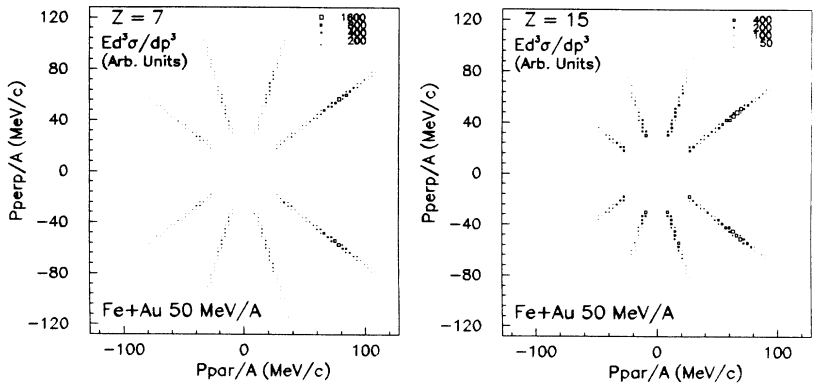

FIG. 9. Inclusive invariant cross section, $E\,d^3\sigma/d^3P$, in the plane $P_{\parallel}$/nucleon versus $P_{\perp}$/nucleon for $Z=7$ and 15. Data are for the 50 MeV/nucleon Fe+Au reaction.

The nucleons are represented by Gaussians of the form

$$f_i(\mathbf{r},\mathbf{p},t)=\frac{1}{(\pi\hbar)^3}\exp\left\{-\frac{[\mathbf{r}-\mathbf{r}_{i0}(t)]^2}{2L}-[\mathbf{p}-\mathbf{p}_{i0}(t)]^2\frac{2L}{\hbar^2}\right\}, \quad (1)$$

where r_{i0} and p_{i0} are the centroid of particle i in coordinate and momentum space. $2L$ is the characteristic width of the wave packet. Note the compatibility of the width in coordinate space $2L$ and the width in momentum space $\hbar^2/2L$ with the uncertainty principle; $2L(h^2/2L)=\hbar^2$. The interactions used here are a local Skyrme two and three particle interaction, a Coulomb and a Yukawa interaction.

With these Gaussian nucleons, the interactions lead to the following Hamiltonian:

$$H=\sum_{i=1}^{N}\frac{\mathbf{p}_i^2}{2m}+\frac{1}{2}\sum_{i,j=1}^{N}{}'\frac{V_{\mathrm{Yuk}}^0}{2|\mathbf{r}_{i0}-\mathbf{r}_{j0}|}(e^L/\gamma_{\mathrm{Yuk}}^2)\left\{e^{-|\mathbf{r}_{i0}-\mathbf{r}_{j0}|/\gamma_{\mathrm{Yuk}}}\left[1-\mathrm{erf}\left[\frac{2L/\gamma_{\mathrm{Yuk}}-|\mathbf{r}_{i0}-\mathbf{r}_{j0}|}{\sqrt{4L}}\right]\right]\right.$$

$$\left.-e^{+|\mathbf{r}_{i0}-\mathbf{r}_{j0}|/\gamma_{\mathrm{Yuk}}}\left[1-\mathrm{erf}\left[\frac{(2L/\gamma_{\mathrm{Yuk}})+|\mathbf{r}_{i0}-\mathbf{r}_{j0}|}{\sqrt{4L}}\right]\right]\right\}$$

$$+\left[\frac{Z}{A}\right]^2\frac{1}{2}\sum_{i,j=1}^{N}{}'\frac{e^2}{|\mathbf{r}_{i0}-\mathbf{r}_{j0}|}\mathrm{erf}\left[\frac{|\mathbf{r}_{i0}-\mathbf{r}_{j0}|}{\sqrt{4L}}\right]$$

$$+\sum_{i=1}^{N}\left[\frac{\alpha}{2}\frac{1}{(4\pi L)^{3/2}\rho_0}\sum_{j=1}^{N}{}'e^{-(\mathbf{r}_{i0}-\mathbf{r}_{j0})^2/4L}+\frac{\beta}{\gamma+1}\left[\frac{1}{(4\pi L)^{3/2}\rho_0}\sum_{j=1}^{N}{}'e^{-(\mathbf{r}_{i0}-\mathbf{r}_{j0})^2/4L}\right]^{\gamma}\right].$$

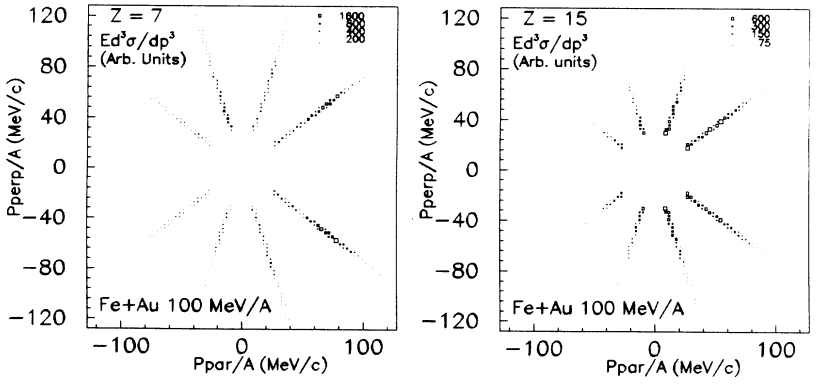

FIG. 10. Same as Fig. 9 for the 100 MeV/nucleon Fe+Au reaction.

The primes on the sums indicate that the self-interaction terms are omitted. The first term is the kinetic energy and the second one is the Yukawa interaction of Gaussian distributed nucleons (1) characterized by its strength $V^0_{\rm Yuk}$. The third term describes the Coulomb interaction of the Gaussian distributed nucleons and the last term denotes the Skyrme interaction, characterized by the parameters α and β. The three-body part of the Skyrme interaction is approximated to be proportional to ρ^γ, in order to allow for the variation of the compressibility of nuclear matter.

The parameters α, β, and γ are adjusted to reproduce the properties of infinite nuclear matter, i.e.,

$$\left.\frac{E}{A}\right|_{\rho=\rho_0} = -16 \text{ MeV} ,$$
$$P=\rho^2 \left.\frac{\partial E/A}{\partial \rho}\right|_{\rho=\rho_0} = 0 \text{ MeV fm}^{-3} , \quad (3)$$
$$K=9\rho^2 \left.\frac{\partial^2 E/A}{\partial \rho^2}\right|_{\rho=\rho_0} = 380 \text{ MeV} .$$

The parameters used here are $\alpha=-124$ MeV, $\beta=70.5$ MeV, $\gamma=2$, $V^0_{\rm Yuk}=-10$ MeV, $\gamma_{\rm Yuk}=1.5$ fm, and $L=2.165$ fm.

The short-range interaction is taken into account in the same way as in the INC and VUU models via a stochastic scattering term: Two nucleons can scatter if the spatial distance of the centroids of their Gaussians is smaller than $\sqrt{\sigma_{\rm tot}/\pi}$. The energy and angular dependence of the experimental differential n-n cross section $d\sigma/d\Omega$ are reproduced. The free n-n cross sections are modified in medium by the Uehling-Uhlenbeck blocking factors $[1-f(r,p)]$, which determine the Pauli blocking probability of the final states in an n-n collision.

For the comparison with the data we used initially the same version of the QMD model as in Ref. [14,15,30] and followed the reaction for 300 fm/c reaction time. However, in order to follow the long-time evolution of the reaction (in particular, the decay of the hot heavy fragments into IMFs) a modified version of the QMD model was developed which includes the Pauli potential of Refs. [50,51]. This new version yields a well defined fermionic ground state of the fragments and, therefore, allows the determination of the excitation energy of the fragments event by event. If the fragments, which are produced in such reactions, are highly excited, they will decay in a time scale (10^{-20} to 10^{-16} sec) which is not available in a molecular dynamical calculation. This secondary decay will modify the results obtained with the original QMD model. In order to investigate the effect of these secondary processes we study a hybrid model, where the first dynamical step is carried out with the modified QMD model (with Pauli potential). After this dynamical step we calculated the excitation energy of each fragment. We then used the statistical multifragmentation model (SMM) of Botvina *et al.* [18,19] for the further decay of the fragments yielding a final theoretical distribution which is compared to the experimental data.

In the calculations presented here we stopped the QMD calculation at 300 fm/c reaction time. At this time the fast preequilibrium emission is finished and the multiplicities and excitation energies are not changing rapidly with time. At this time the central density of the excited fragments produced within the QMD model is about one-half of the nuclear matter density. This is in good agreement with the freeze-out density used in the SMM model. In the SMM model the freeze-out volume V_F is not a fixed parameter, but depends on the multiplicity M of the fragmentation channel in the form

$$V_F=(1+\chi)V_0, \quad \chi=\left[1+\frac{d}{R_0}(M^{1/3}-1)\right]^3-1 ,$$

with $d=1.4$ fm and $R_0=1.17A_0^{1/3}$ fm. For a typical decay channel ($A_0=100$, $M=10$) this yields a freeze-out volume $V_F\approx 2V_0$.

V. QMD CALCULATIONS AND COMPARISON TO DATA

Figures 11–14 show comparisons between data and QMD calculations without the Pauli potential for charge and angular distributions. The calculations with this original QMD were performed for 1900 events at 50 MeV/nucleon and 1800 events at 100 MeV/nucleon. The theoretical events have been calculated with random impact parameters in the range 0–12 fm and have been geometrically weighted. The indicated error bars are of statistical origin only.

The calculated differential cross sections were normalized to the total reaction cross section (σ_R) for the Fe+Au reaction calculated as a function of energy and impact parameter [52] ($\sigma_R=3.95$ b at 50 MeV/nucleon

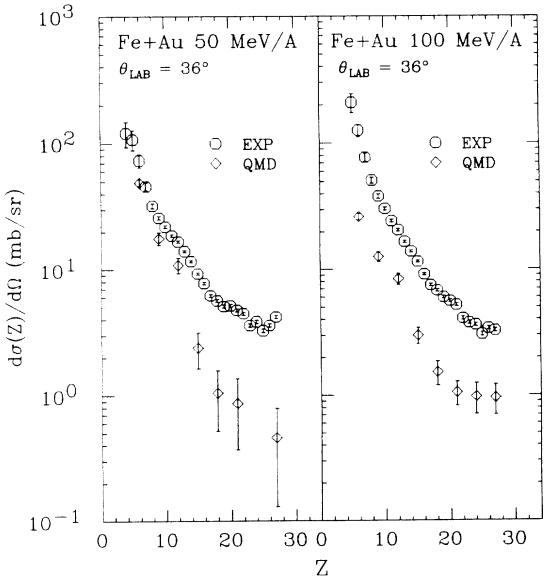

FIG. 11. Comparison of experimental and theoretical charge distributions at a laboratory angle of 36° for the 50 and 100 MeV/nucleon Fe+Au reaction. The theoretical calculations are from the QMD model without the Pauli potential or subsequent SMM deexcitation. The experimental distributions have been corrected for MWPC efficiency as described in the text.

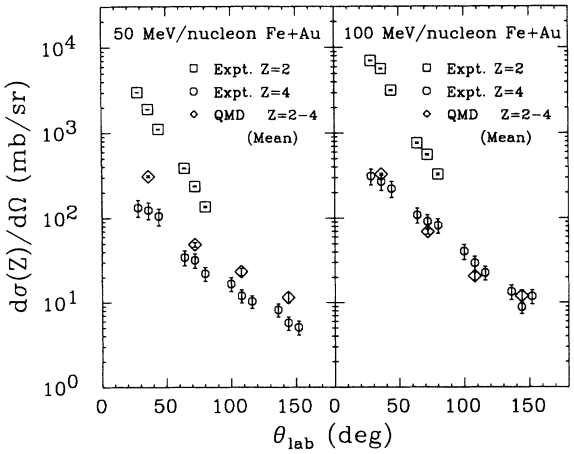

FIG. 12. Comparison of experimental and theoretical angular distributions for the 50 and 100 MeV/nucleon Fe+Au reactions. Data are for $Z=2$ and 4. Calculations are summed for the interval $Z=2$ to 4. The theoretical calculations are from the QMD model without the Pauli potential or subsequent SMM deexcitation.

and $\sigma_R = 4.24$ b at 100 MeV/nucleon). In addition, calculations were subjected to the same low energy cutoffs that are present in the data set.

The comparisons indicate that the calculated and experimental Z distributions have roughly the same shape but the QMD yields are lower than experimentally observed. The angular distributions are, however, very different. The original QMD calculations are more sharply forward peaked and the effect is accentuated at higher Z and for the lower bombarding energy (50 MeV/nucleon). At the most forward angles the absolute comparison of cross sections is quite reasonable.

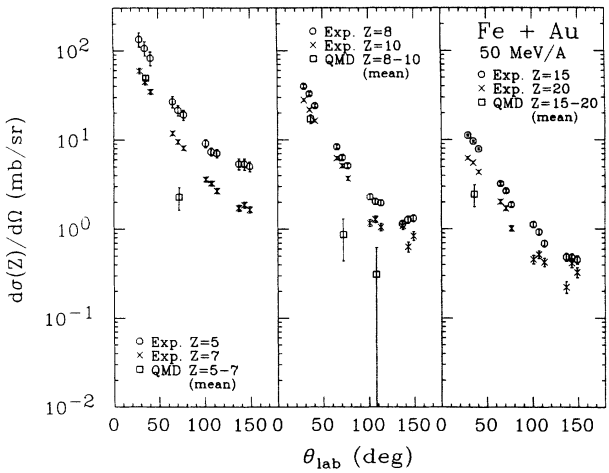

FIG. 13. Comparison of experimental and theoretical angular distributions for the 50 MeV/nucleon Fe+Au reaction. Data are for the single charge values $Z=5$, 7, 8, 10, 15, and 20. Calculations are summed for the intervals $Z=5$ to 7, 8 to 10, and 15 to 20. The theoretical calculations are from the QMD model without the Pauli potential or the subsequent SMM deexcitation.

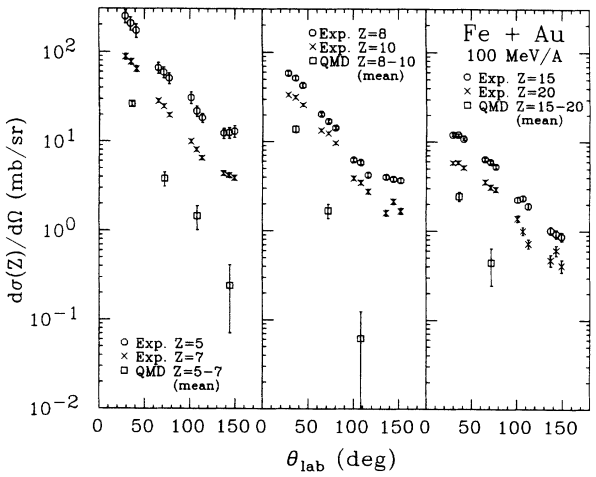

FIG. 14. Same as Fig. 13 for the 100 MeV/nucleon Fe+Au reaction.

The original QMD model treats the early stages of the collision in reasonable detail and should yield a good prediction of the initial fragmentation of the system. However, as discussed in the previous section, this model neglects the subsequent deexcitation of the fragments. This neglect leads to the large discrepancies between the model and the experimental data since the fragments formed in the initial dynamical part of the collision decay further before being observed in the experimental acceptance [53]. In our experiment the primary IMF source is the multifragmentation of the target residue. Thus, the discrepancy between data and original QMD in Figs. 13 and 14 is most likely explained by the decay of such a source which is not included in the model.

In the original version of the QMD model it is not possible to test this hypothesis because the ground states of the final fragments are not well enough determined for a reliable estimate of their excitation energies. However, the improved QMD model utilizing a momentum-dependent potential (Pauli potential) to simulate the Pauli exclusion principle has shown considerable promise for overcoming this problem. Recent calculations [51] have demonstrated the ability of this approach to produce clustering in low density nuclear matter and to adequately reproduce the radii and binding energies for finite nuclear systems. As discussed above in Sec. IV, this new version of QMD has now been expanded to calculate the temperatures of the emitted fragments and coupled to the statistical multifragmentation model (SMM) developed previously by Botvina *et al.* [18,19]. The details of this model and comparisons to a broad selection of data will be published elsewhere [54]. In this paper we show results from these hybrid calculations as applied to the Fe+Au case.

Figures 15 and 16 show comparisons of the inclusive charge distributions at the four angular intervals centered at 36°, 72°, 108°, and 144°. The data show little variation with bombarding energy at the most forward angle which dominates the cross section. There are, however, increases in yield of factors of 2–3 at the more backward angles and the higher bombarding energy.

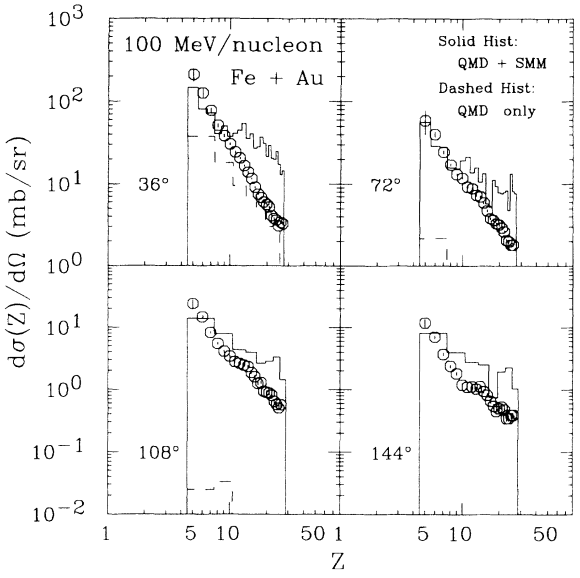

FIG. 15. Charge yields for the 100 MeV/nucleon Fe+Au reaction at the angular intervals noted. The circles represent the experimental data while the histograms represent results from the modified QMD model alone (dashed) and from the QMD with secondary decay included via the SMM model (solid).

Also shown in Figs. 15 and 16 are calculated results for the full range of impact parameters ($b=0-12$ fm) obtained with the modified QMD model alone (dashed histograms) and after the secondary decay is included utilizing the SMM model (full histograms). An efficiency cut has been applied to the calculations to reproduce the experimental velocity cutoff at 1 cm/nsec. Within limited statistical accuracy, the calculations reproduce the measured velocity spectra shown in Figs. 7 and 8 reasonably well except for the lightest fragments at the most forward angle where the calculated spectra are somewhat harder. At backward angles where threshold effects are most important the calculated and measured spectra agree very well.

For central collisions the average excitation energies of the primordial heavy fragments ($A>10$) are about 5–6 MeV/nucleon. As the collisions become more peripheral the masses of the heaviest remnants increase but their average excitation energy decreases steadily. After the secondary decay the model produces significant yields at backward angles and approximately reproduces the data.

These comparisons show that at backward angles all of the observed IMFs stem from the secondary decay of large highly excited target remnants. This can also be seen in Figs. 17 and 18 where we compare the angular distributions for specific Z intervals. The modified QMD model shows significant yields only at the most forward angles. At backward angles the IMF yield comes entirely from the decay of the excited target residue. For the angular distributions of prompt fragments the modified QMD model gives very similar results to those obtained with the previous version (see Figs. 13 and 14). This indicates that the addition of the Pauli potential does not influence the dynamics of the reaction.

A comparison between the two bombarding energies in Figs. 15–18 indicates that the hybrid model overestimates the fragment yield by at least a factor of 2 at the lower energy. This is probably due to the sensitivity of the final fragment distribution from the SMM stage to the initial excitation energy of the primordial QMD; the uncertainty in the calculated QMD excitation energy is of order 1 MeV/nucleon. In addition, the free volume available for translational motion of the fragment is the only free parameter in the SMM model. For the calculations presented in Figs. 15–18, the freeze-out density has been taken to be half normal nuclear matter density. Although this value has been successfully used to describe

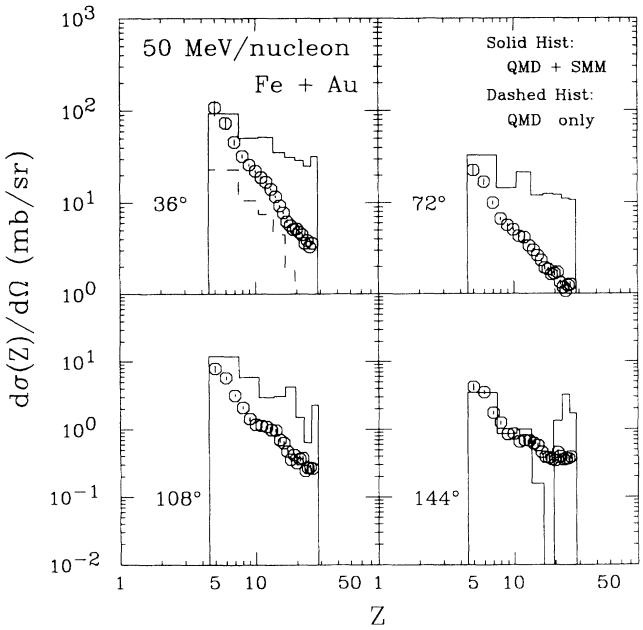

FIG. 16. Same as Fig. 15 for the 50 MeV/nucleon Fe+Au reaction.

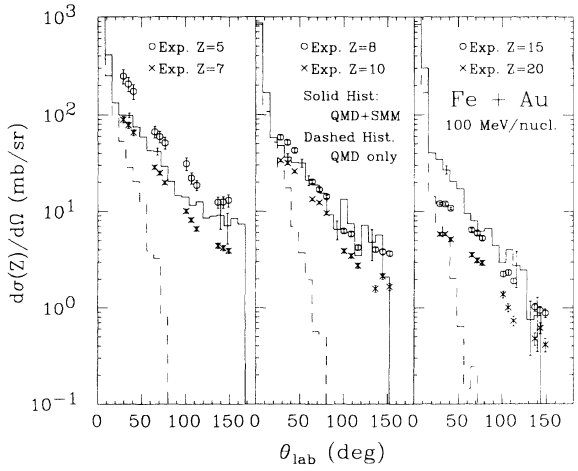

FIG. 17. Angular distributions for the 100 MeV/nucleon Fe+Au reaction and various charge intervals. The symbols represent the experimental data; the histograms represent results from the modified QMD model alone (dashed) and from the QMD with secondary decay included via the SMM model (solid).

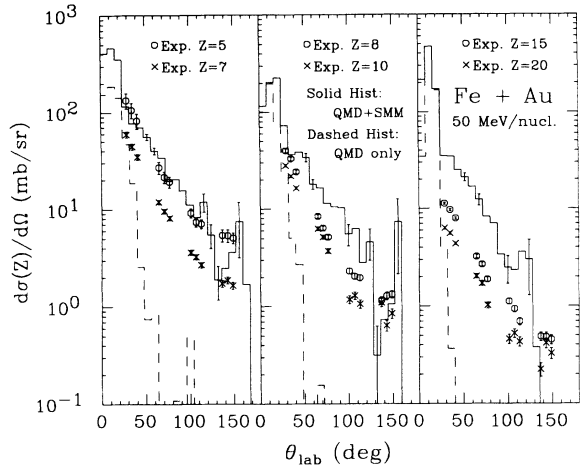

FIG. 18. Same as Fig. 17 for the 50 MeV/nucleon Fe+Au reaction.

multifragmentation in proton-induced reactions [19], the density of the decaying primordial fragments in heavy ion collisions may be different.

A more detailed study of this model and its application to the multiparticle correlations available in this date set is in progress and will be reported at a later time. It should be noted that Colonna *et al.* [23] have recently reported preliminary results at intermediate energies from a similar two-step calculational approach using the Boltzmann-Norheim-Vlasov (BNV) equation [55] to simulate the early dynamical evolution of the heavy ion collision and the statistical decay code GEMINI [56] to handle the deexcitation. Their conclusions are generally consistent with the results presented in this paper.

VI. DISCUSSION

We conclude from the comparisons of experimental data with the results from the QMD+SMM model that a complete treatment of the reaction using QMD with the Pauli potential for the initial dynamics and SMM for the late time decay is in good agreement with the data.

Previous analysis of 50, 75, and 100 MeV/nucleon Nb+Au data [4] acquired using the PAGODA detector array has shown that the IMF production cross sections, angular distributions, and multiplicities are virtually identical for all three Nb energies as well as for the 100 MeV/nucleon Fe+Au data. However, the IMF cross sections show a significant decrease for the 50 MeV/nucleon Fe+Au reaction. This behavior is qualitatively consistent with the idea of limiting fragmentation in which the observed fragment production systematics become independent of the entrance channel above a threshold energy. For these systems, the center-of-mass energy increases from 2.2 to 6.3 GeV for the 50 MeV/nucleon Fe and 100 MeV/nucleon Nb projectiles, respectively. As the energy available for excitation increases beyond the total binding energy of the system, it would be reasonable to expect a limit to the increase in IMF cross sections as the most central collisions begin leading to a complete disintegration into light particles and the impact parameters feeding IMF production begin to increase. A similar line of reasoning has been offered by the ALADIN group [9] to explain the remarkable target dependence of the IMF multiplicity observed with a 600 MeV/nucleon Au beam on a variety of light and heavy targets. One result of this limiting behavior is that the excitation energy range feeding IMF production should become relatively independent of the bombarding energy above the IMF threshold region in a manner similar to that observed for fission decay in higher energy reactions [27]. This may be the most reasonable explanation for the apparent limiting temperature observed in several contexts in intermediate energy heavy ion collisions [10–13].

VII. SUMMARY

We have presented a comprehensive set of experimental results on the production of intermediate mass fragments from bombardments of a Au target by Fe beams at 50 and 100 MeV/nucleon. The results are compared to predictions of a quantum molecular dynamics model and the first quantitative results on the effects of adding a statistical deexcitation stage to this model are presented.

Both the experimental systematics and the comparisons to QMD calculations indicate that the large cross section for IMF emission at large angles is due to the multifragmentation of the excited heavy residue that remains following the initial stage of the interaction. First results from an expanded model coupling QMD to a multifragmentation-evaporation calculation indicate that this approach can qualitatively reproduce the measured distributions. Further work is in progress.

ACKNOWLEDGMENTS

We are pleased to acknowledge the help of the LBL Bevalac staff in supporting these experiments. We would also like to acknowledge the hard work of Ron Marquardt (MIT) and James Larkin (CalState, Hayward). One of us (H.C.B.) gratefully acknowledges support from the Alexander von Humbolt-Stiftung and the hospitality of the Institute fur Theoretische Physik der University Frankfurt during the preparation of this manuscript. This work was performed under the auspices of the U.S. Department of Energy by the Lawrence Livermore National Laboratory under Contract No. W-7405-Eng-48, by the Los Alamos National Laboratory under Contract No. W-7405-ENG-36, by the Lawrence Berkeley Laboratory under Contract No. DE-AC03-76SF00098, and by Argonne National Laboratory under Contract No. W-31-109-ENG-38.

[1] L. G. Sobotka, M. L. Padgett, G. J. Wozniak, G. Guarino, A. J. Pacheco, L. G. Moretto, Y. Gu, and R. G. Stokstad, Phys. Rev. Lett. **51**, 2187 (1983); L. G. Sobotka, M. A. McMahan, R. J. McDonald, C. Signarbieux, G. J. Wozniak, M. L. Padgett, Y. Gu, Z. H. Liu, Z. Q. Yao, and L. G. Moretto, *ibid.* **53**, 2004 (1984).

[2] K. G. R. Doss, H. A. Gustafsson, H. Gutbrod, J. W. Harris, B. V. Jacak, K. H. Kampert, B. Kolb, A. M.

Poskanzer, H. G. Ritter, H. R. Schmidt, L. Teitelbaum, M. Tincknel, S. Weiss, and H. Weiman, Phys. Rev. Lett. **59**, 2720 (1987).

[3] N. T. Porile, A. J. Bujak, D. D. Carmony, Y. H. Chung, L. J. Gutay, A. S. Hirsch, M. Mahi, G. L. Paderewski, T. C. Sangster, R. P. Scharenberg, and B. C. Stringfellow, Nucl. Phys. **A471**, 149 (1987); Phys. Rev. C **39**, 1914 (1989).

[4] D. J. Fields, T. C. Sangster, M. L. Webb, B. A. Remington, H. C. Britt, L. F. Hansen, R. G. Lanier, D. Massoletti, M. N. Namboodiri, G. L. Struble, M. L. Begemann-Blaich, T. Blaich, M. M. Fowler, J. Wilhelmy, S. Kaufman, F. Videbaek, Y. D. Chan, A. Dacal, A. Harmon, J. Pouliot, R. Stokstad, and Z. Fraenkel, Nucl. Phys. **A495**, 209c (1989); M. N. Namboodiri *et al.*, in *Nuclear Dynamics and Nuclear Disassembly,* edited by J. B. Natowitz (World Scientific, Singapore, 1990), p. 449; H. C. Britt *et al.*, in *The Nuclear Equation of State Part A,* Vol. 216A of *NATO ASI Series B: Physics,* edited by W. Griener and H. Stöcker (Plenum, New York, 1989), p. 177.

[5] K. Alecklett, L. Sihver, and W. Loveland, Phys. Lett. B **197**, 34 (1987).

[6] R. Trockel, U. Lynen, J. Pochodzalla, W. Trautmann, N. Brummund, E. Eckert, R. Glasov, K. D. Hildenbrand, K. H. Kampert, W. F. J. Muller, D. Pelte, H. J. Rabe, H. Sann, R. Santo, H. Stelzer, and R. Wada, Phys. Rev. Lett. **59**, 2844 (1987); R. Trockel, K. D. Hildebrand, U. Lynen, W. F. J. Muller, H. J. Rabe, H. Sann, H. Stelzer, W. Trautmann, R. Wada, E. Eckert, J. Pochodzalla, and N. Brummund, Phys. Rev. C **39**, 729 (1989).

[7] A. I. Warwick, H. H. Weiman, H. H. Gutbrod, M. R. Maier, J. Peter, H. G. Ritter, H. Stelzer, F. Weik, M. Friedman, D. J. Henderson, S. B. Kaufman, E. P. Steinberg, and B. D. Wilkins, Phys. Rev. C **27**, 1083 (1983).

[8] R. J. Charity, M. A. McMahan, G. J. Wozniak, R. J. McDonald, L. G. Moretto, D. G. Sarantites, L. G. Sobotka, G. Guarino, A. Pantaleo, L. Fiore, A. Gobbi, and K. D. Hildenbrand, Nucl. Phys. **A483**, 371 (1988).

[9] C. A. Ogilvie, J. C. Adloff, M. Begemann-Blaich, P. Bouissou, J. Hubele, G. Imme, I. Iori, P. Kreutz, G. J. Kunde, S. Leray, V. Lindenstruth, Z. Liu, U. Lynen, R. J. Meijer, U. Milkau, A. Moroni, W. F. J. Muller, C. Ngo, J. Pochodzalla, G. Raciti, G. Rudolf, H. Sann, A. Schuttauf, W. Seidel, L. Stuttge, W. Trautmann, and A. Tucholski, Phys. Rev. Lett. **67**, 1214 (1991); J. Hubele *et al.*, Gesellschaft für Schwerionenforschung, Darmstadt, Germany, Report GSI-91-33, 1991.

[10] J. Pochodzalla, C. K. Gelbke, W. G. Lynch, M. Maier, D. Ardouin, H. Delagrange, H. Doubre, C. Gregoire, A. Kyanowski, W. Mittig, A. Peghaire, J. Peter, F. Saint-Laurent, and B. Zwieglinski, Phys. Rev. C **35**, 1695 (1987); C. B. Chitwood, C. K. Gelbke, J. Pochodzalla, Z. Chen, D. J. Fields, W. G. Lynch, R. Morse, M. B. Tsang, D. H. Boal, and J. C. Shillcock, Phys. Lett. B **172**, 27 (1986); Z. Chen, C. K. Gelbke, J. Pochodzalla, C. B. Chitwood, D. J. Fields, W. G. Lynch, and M. B. Tsang, *ibid.* **199**, 71 (1987).

[11] G. J. Kunde, J. Pochodzalla, J. Aichelin, E. Berdermann, B. Berthier, C. Cerruti, C. K. Gelbke, J. Hubele, P. Kreutz, S. Leray, R. Lucas, U. Lynen, U. Milkau, W. F. J. Muller, C. Ngo, C. H. Pinkenburg, G. Raciti, H. Sann, and W. Trautmann, Gesellschaft für Schwerionenforschung, Darmstadt, Germany, Report GSI-91-17, 1991.

[12] D. X. Jiang, H. Doubre, J. Galin, D. Guerreau, E. Piasecki, J. Pouthas, A. Sokolov, B. Cramer, G. Ingold, U. Jahnke, E. Schwinn, J. L. Charvet, J. Frehaut, B. Lott, C. Magnago, M. Morjean, Y. Patin, Y. Pranal, J. L. Uzureau, B. Gatty, and D. Jacquet, Nucl. Phys. **A503**, 560 (1989).

[13] J. Galin, Grand Accélérateur National d'Ions Lourds, Caen CEDEX, France, Report P9017.

[14] J. Aichelin, G. Peilert, A. Bohnet, A. Rosenhauer, H. Stöcker, and W. Greiner, Phys. Rev. C **37**, 2451 (1988).

[15] G. Peilert, A. Rosenhauer, J. Aichelin, H. Stöcker, and W. Greiner, Mod. Phys. Lett. A **3**, 459 (1988); Phys. Rev. C **39**, 1402 (1989).

[16] G. Fai and J. Randrup, Nucl. Phys. **A381**, 557 (1982); **A404**, 551 (1983).

[17] D. H. E. Gross, L. Satpathy, Meng Ta-chung, and M. Satpathy, Z. Phys. A **309**, 41 (1982); Nucl. Phys. **A428**, 313 (1984).

[18] J. P. Bondorf, R. Donangelo, I. N. Mishustin, C. J. Pethick, H. Shulz, and K. Sneppen, Nucl. Phys. **A443**, 321 (1985); **A444**, 460 (1985); **A448**, 753 (1986).

[19] A. S. Botvina, A. S. Ijinov, I. N. Mishustin, J. P. Bondorf, R. Donangelo, and K. Sneppen, Nucl. Phys. **A475**, 663 (1987); **A507**, 649 (1990).

[20] D. Hahn and H. Stöcker, Nucl. Phys. **A476**, 718 (1988).

[21] M. Blann, Phys. Rev. Lett. **54**, 2215 (1985); Phys. Rev. C **32**, 1231 (1985); M. Blann, T. Komoto, and I. Tserruya, *ibid.* **40**, 2498 (1989); M. Blann, M. G. Mustafa, G. Peilert, H. Stöcker, and Walter Greiner, *ibid.* **44**, 431 (1991).

[22] C. Barbagallo, J. Richert, and P. Wagner, Z. Phys. A **324**, 97 (1986).

[23] M. Colonna, P. Roussel-Chomaz, N. Colonna, M. Di Toro, L. G. Moretto, and G. J. Wozniak, LBL Report LBL-30810, 1991.

[24] K. Sneppen and L. Vinet, Nucl. Phys. **A480**, 342 (1988).

[25] T. Blaich, M. Begemann-Blaich, M. M. Fowler, J. B. Wilhelmy, H. C. Britt, D. J. Fields, L. F. Hansen, M. N. Namboodiri, T. C. Sangster, and Z. Fraenkel, Phys. Rev. C **45**, 689 (1992).

[26] M. M. Fowler, T. C. Sangster, M. L. Begemann-Blaich, T. Blaich, J. A. Boissevain, H. C. Britt, Y. D. Chan, A. Dacal, D. J. Fields, Z. Fraenkel, A. Gavron, A. Harmon, B. V. Jacak, R. G. Lanier, P. S. Lysaght, G. Mamane, D. J. Massoletti, M. N. Namboodiri, J. Pouloit, R. G. Stokstad, M. L. Webb, and J. B. Wilhelmy, Nucl. Instrum. Methods A **281**, 517 (1989).

[27] M. L. Begemann-Blaich, Th. Blaich, M. M. Fowler, J. B. Wilhelmy, H. C. Britt, D. J. Fields, L. F. Hansen, R. G. Lanier, D. J. Massoletti, M. N. Namboodiri, B. A. Remington, T. C. Sangster, G. L. Struble, M. L. Webb, Y. D. Chan, A. Dacal, A. Harmon, J. Pouliot, R. G. Stokstad, S. Kaufman, F. Videbaek, and Z. Fraenkel, Phys. Rev. C **45**, 677 (1992).

[28] J. Aichelin and H. Stöcker, Phys. Lett. B **176**, 14 (1986).

[29] J. Aichelin, Phys. Rep. **202**, 233 (1991).

[30] M. Berenguer, C. Hartnack, G. Peilert, A. Rosenhauer, W. Schmidt, J. Aichelin, H. Stöcker, and W. Greiner, J. Phys. G **18**, 655 (1992).

[31] H. Kruse, B. V. Jacak, and H. Stöcker, Phys. Rev. Lett. **54**, 289 (1985).

[32] J. J. Molitoris and H. Stöcker, Phys. Rev. C **32**, 346 (1985); Phys. Lett **162B**, 47 (1985).

[33] H. Kruse, B. V. Jacak, J. J. Molitoris, G. D. Westfall, and H. Stöcker, Phys. Rev. C **31**, 1770 (1985).

[34] J. J. Molitoris, H. Stöcker, and B. L. Winer, Phys. Rev. C **36**, 220 (1987).

[35] C. Gregoire, B. Remaud, F. Sebille, and L. Vinet, Nucl. Phys. **A465**, 317 (1987).
[36] G. F. Bertsch, H. Kruse, and S. Das Gupta, Phys. Rev. C **29**, 673 (1984).
[37] J. Aichelin and H. Stöcker, Phys. Lett. **163**, 59 (1985).
[38] J. Aichelin and G. F. Bertsch, Phys. Rev. C **31**, 1730 (1985).
[39] C. Gale, G. F. Bertsch, and S. Das Gupta, Phys. Rev. C **35**, 1666 (1987).
[40] G. F. Bertsch, W. G. Lynch, and M. B. Tsang, Phys. Lett. B **189**, 384 (1987).
[41] A. Bodmer and C. N. Panos, Phys. Rev. C **15**, 1342 (1977).
[42] L. Wilets, E. M. Henley, M. Kraft, and A. D. Mackellar, Nucl. Phys. **A282**, 341 (1977).
[43] L. Wilets, Y. Yariv, and R. Chestnut, Nucl. Phys. **A301**, 359 (1978).
[44] D. J. E. Callaway, L. Wilets, and Y. Yariv, Nucl. Phys. **A327**, 250 (1979).
[45] A. R. Bodmer, C. Panos, and A. D. MacKellar, Phys. Rev. C **22**, 1025 (1980).
[46] J. J. Molitoris, J. B. Hoffer, H. Kruse, and H. Stöcker, Phys. Rev. Lett. **53**, 899 (1984).
[47] S. M. Kiselev and Yu. E. Pokroskil, Yad. Fiz. **38**, 82 (1983) [Sov. J. Nucl. Phys. **38**, 46 (1983)].
[48] S. M. Kiselev, Yad. Fiz. **39**, 32 (1984) [Sov. J. Nucl. Phys. **39**, 18 (1984)].
[49] S. M. Kiselev, Yad. Fiz. **44**, 946 (1986) [Sov. J. Nucl. Phys. **44**, 610 (1986)].
[50] C. Dorso, S. Duarte, and J. Randrup, Phys. Lett. B **188**, 287 (1987); C. Dorso and J. Randrup, *ibid.* **215**, 611 (1988); **232**, 29 (1989).
[51] G. Peilert, J. Randrup, H. Stöcker, and W. Greiner, Phys. Lett. B **260**, 271 (1991).
[52] S. Kox, A. Gamp, R. Cherkaqui, A. J. Cole, N. Longequeue, J. Menet, C. Perrin, and J. B. Viano, Nucl. Phys. **A420**, 162 (1984); Y. El Masri, F. Hanappe, G. Costa, J. F. Bruandet, S. Kox, A. C. Mueller, and R. Bimbot, in *Proceedings of the Symposium in Nuclear Dynamics and Nuclear Disassembly,* Dallas, Texas, 1989, edited by J. B. Natowitz (World Scientific, Singapore, 1990), p. 42.
[53] M. Blann, M. G. Mustafa, G. Peilert, H. Stöcker, and W. Greiner, University of California, Lawrence Livermore National Laboratory Report UCRL-JC-106767, 1991; Phys. Rev. C **44**, 431 (1991).
[54] G. Peilert, J. Konopka, H. Stöcker, W. Greiner, M. Blann, and M. G. Mustafa, Phys. Rev. C (in press).
[55] A. Bonasera, G. F. Burgio, and M. Di Toro, Phys. Lett. B **221**, 233 (1989); A. Bonasera, G. Russo, and H. H. Wolter, *ibid.* B **246**, 337 (1990).
[56] R. J. Charity *et al.*, Nucl. Phys. **A453**, 371 (1988); D. R. Bowman *et al.*, *ibid.* **A523**, 386 (1991).